Stress Changes Before and During the Pu‘u ‘Ō‘ō-Kūpaianaha Eruption

By James H. Dieterich, Valérie Cayol, *and* Paul Okubo

Abstract

Surface deformation and earthquake data for Kīlauea Volcano have been analyzed as they pertain to stress interactions before and during the Pu‘u ‘Ō‘ō-Kūpaianaha eruption. A newly developed method was used to solve for Coulomb stress changes from earthquake rate changes that facilitates quantitative comparisons between earthquake and deformation data sets. Between the 1975 M7.2 Kalapana earthquake and the start of the Pu‘u ‘Ō‘ō-Kūpaianaha eruption in 1983, deformation rates of Kīlauea Volcano were the most rapid ever recorded. During this period, deformation was characterized by expansion of a dike-like magma system within Kīlauea's rift zones, coupled with aseismic creep over a narrow zone of a low-angle fault located beneath the volcano's south flank. For the 1976–83 period, the rate of rift opening is estimated to have averaged 40 cm per year on the basis of ground deformation. At the onset of the Pu‘u ‘Ō‘ō-Kūpaianaha eruption in January 1983, the dike propagated to the surface to form the eruptive fissures. Deformation data and seismicity stress solutions indicate that a fivefold slowing of stressing rates in Kīlauea's south flank occurred either in late 1979 or at the start of the of Pu‘u ‘Ō‘ō-Kūpaianaha eruption in January 1983, depending on location. The stressing rates before and after the onset of the eruption are consistent with changes in volume of magma stored before and after the onset of the Pu‘u ‘Ō‘ō-Kūpaianaha eruption.

Introduction

Seismic activity often signals the occurrence of magmatic processes within volcanoes, such as the intrusion of new magma bodies and the inflation, or deflation, of existing bodies. Indeed, major volcanic events are often associated with large earthquakes or, in extreme cases, edifice collapse. The intimate association of seismicity with volcanic activity indicates that interactions between faulting and magma bodies are a fundamental aspect of volcanic processes. Stress changes induced by magmatic processes can drive faulting and earthquake activity. Conversely, faulting, by relieving stresses from previous intrusive processes, can establish stress states favorable to new or continued intrusion. That is, faulting can create "room" to accommodate the added volume of intruded magma.

At Kīlauea, these interactions are very evident. Changes of seismic activity characterize the onset of eruptions and are primary indicators of subsurface movements of magma (Klein and others, 1987). Additionally, interactions between rift-zone magmatic expansion and detachment faulting at the base of the volcano appear to underlie both the formation and the persistence of Kīlauea's rift zones (Dieterich, 1988).

This paper presents a combined analysis of deformation and earthquake rates data related to the Pu‘u ‘Ō‘ō-Kūpaianaha eruption. Its focus is the south flank of Kīlauea and the adjacent east rift zone in the region of the Pu‘u ‘Ō‘ō-Kūpaianaha eruptive fissures (fig. 1). The work attempts to identify and delineate stress interactions within the south flank of Kīlauea and to develop a consistent model of magmatic and earthquake processes within Kīlauea particularly as they relate to the Pu‘u ‘Ō‘ō-Kūpaianaha eruption.

The analysis includes the period following the M7.2 Kalapana earthquake in 1975 and continues through the onset of the Pu‘u ‘Ō‘ō-Kūpaianaha eruption in 1983. The 1975 Kalapana earthquake marks a point of major change in the behavior of Kīlauea. In the 15 years before that earthquake, eruptive activity was prevalent, but from the 1975 Kalapana earthquake to the 1983 eruption, magmatic activity was predominately intrusive (Dzurisin and others, 1984). The interval between the 1975 earthquake and the onset of the Pu‘u ‘Ō‘ō-Kūpaianaha eruption was also a period of exceptionally rapid deformation (fig. 2) and intense seismic activity (fig. 1), with extension rates across Kīlauea caldera averaging about 25 cm/yr. Following the onset of the 1983 Pu‘u ‘Ō‘ō-Kūpaianaha eruption, activity changed from intrusion to nearly continuous rift eruption, and deformation rates decreased to about 4 cm/yr (Delaney and others, 1998).

Model of Kīlauea's Rift Zone and South Flank

Previous investigations have identified the principal structural elements of Kīlauea Volcano. Geodetic and seismologic observations (for example, Fiske and Kinoshita, 1969; Klein and others, 1987) indicate that magma rises from the mantle

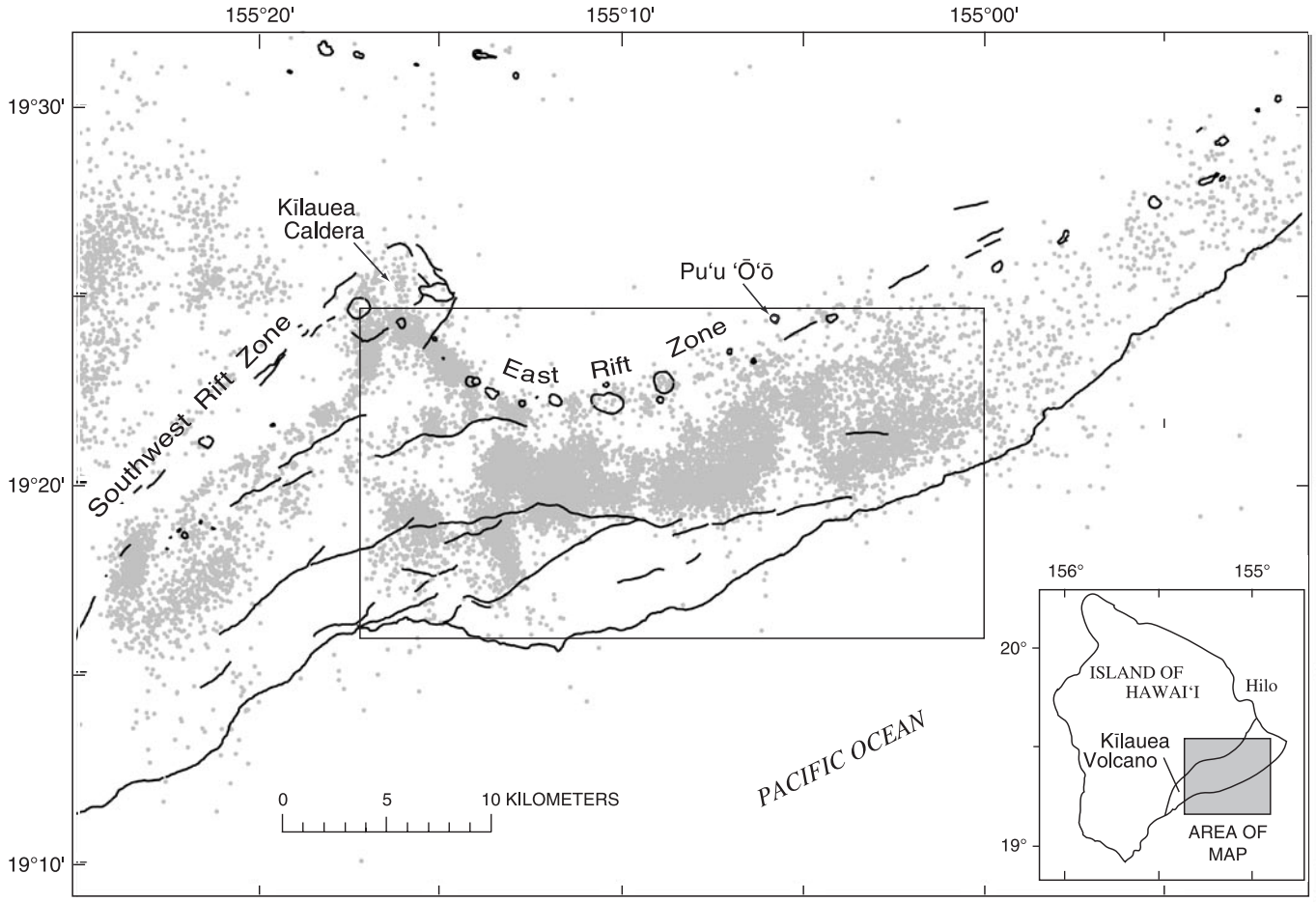

Figure 1. Map showing principal features of Kīlauea Volcano. Study area for analysis of the seismicity data (inner rectangle) consists of the east rift zone (including the Pu'u 'Ō'ō-Kūpaianaha eruption site) and the seismically active south flank of Kīlauea. Black lines are faults; open circles are volcanic craters. Earthquake locations, M≥2, recorded from 1976 to 1982, are shown by gray dots.

through a conduit located below Kīlauea's summit. From the summit region, magma is then laterally supplied to Kīlauea's two rift zones—the east and the southwest rift zones (fig. 1). Magma is stored within these rift zones, as evidenced from petrologic data (Wright and Fiske, 1971) and geophysical studies (Hill and Zucca, 1987; Okubo and others, 1997). Precise relative relocations of shallow rift earthquakes (Gillard and others, 1996; Rubin and others, 1998) define narrow ribbons that are interpreted to mark the highly stressed zone at the top of a vertical tabular magma reservoir. This observation, together with the long wavelength of deformations across the rift system (Delaney and others, 1990), suggest the dilation of a dike-like reservoir that extends from a depth of about 3 km downward to the pre-volcano sea floor, which is depressed to a depth of 9 to 10 km beneath sea level in the vicinity of the rift zones (fig. 3). The continuous deformation at sites widespread on the volcano indicates that the injection of magma into the deep rift zones is a steady process (Delaney and others, 1990). In addition, supply of magma to the rift zones is sometimes accompanied by swarms of shallow (1–4 km) earthquakes corresponding to the rapid intrusion of shallow dikes, which may lead to the formation of eruptive fissures (Klein and others, 1987).

Geodetic monitoring provides a number of data sets that record the surface deformations of Kīlauea's rift zones and flank. In the present study, we model trilateration, leveling, and sea-level data using a three-dimensional mixed boundary element method that takes topography into account (Cayol and Cornet, 1998). This method employs stress boundary conditions and permits simultaneous representation of stress interactions among the faults and magma bodies that make up the structural elements of Kīlauea. The medium is assumed to be elastic.

The southwest and east rift zones are represented as a single steeply dipping dike that extends to the base of the volcano (fig. 3). The horizontal location of the dike is defined by shallow seismicity along the rift zones and by the locus of maximum subsidence, determined by leveling. Where available at the time of the study, relocated earthquakes (Gillard and others, 1996; Rubin and others, 1998) were used. In the boundary element model, rift zone expansion occurs by intrusion of magma into the rift zones (Swanson and others, 1976) and is coupled to, and accommodated by, fault slip at the interface between the volcano and the pre-existing sea floor (Nakamura, 1982, Dieterich, 1988). Evidence for a decollement at the base

of the volcano is provided by the 1975 M7.2 and the 1989 M6.1 earthquakes, which were caused by seaward motion on a low-angle fault (Ando, 1979; Bryan, 1992), probably located at the interface between the volcanic edifice and the depressed former sea floor. Additionally, high rates of seismicity at depths ranging from 6 to 12 km characterize the south flank of Kīlauea. Relative relocations (Got and others, 1994) showed that some of the earthquakes reveal a low-angle, northward dipping fault corresponding to the base of the edifice.

The starting model assumes that this low-angle fault is located at 9-km depth at the rift zones. Results presented below indicate that the scarcity of earthquakes close to the rift zones is probably related to aseismic fault creep of the fault. This could be caused by elevated temperatures in the rift system, which favor fault creep (Tse and Rice, 1986), and possibly by the creep of hot, olivine-rich magma and olivine cumulates, which may be present at the base of the rifts (Clague and Denlinger, 1994). Consequently, the fault in the starting model is allowed to slip over a narrow area corresponding to the aseismic region south of the rift zones (fig. 3). The dip of this fault is assumed to be 5° to the northwest, a compromise between various independent estimates (Got and others, 1994; Crosson and Endo, 1982; Thurber and Gripp, 1988). The boundary conditions are stresses. All parts of the rift system are assumed to be hydraulically connected, resulting in a single overpressure for the dike. The fault is assumed to move passively in response to the reservoir dilation and, consequently, has a null stress perturbation. Young's modulus is taken at 50 GPa, a value deduced from the P-wave velocity in the south flank (Okubo and others, 1997) and corrected by a factor of 0.7 to account for the difference between the static and dynamic modulus at a confining pressure of 100 MPa (Cheng and Johnston, 1981). Poisson's ratio is assumed to be 0.25.

Model variables are the depth, height, width, dip, and opening of the rift-zone dike, the dip and depth of the low-angle fault, and the width of the creeping portion of the fault adjacent to the rifts. The two principal outputs of the model are (1) predicted surface deformations, and (2) stress changes within Kīlauea. To compare among the deformation solutions, the error χ^2 was computed on relative displacements along the trilateration baselines (Cayol and others, 2000). The indeterminate components of the velocity field are adjusted using the model coordinate method of network adjustment (Segall and Matthews, 1988). The stress solutions are compared with the results of the seismicity analysis.

Analysis of Earthquake Rate Data

For analysis of seismicity data, a recently developed method (Dieterich and others, 2000) was employed that uses seismicity rate changes to determine changes of stress. That study presented preliminary results from Kīlauea and made

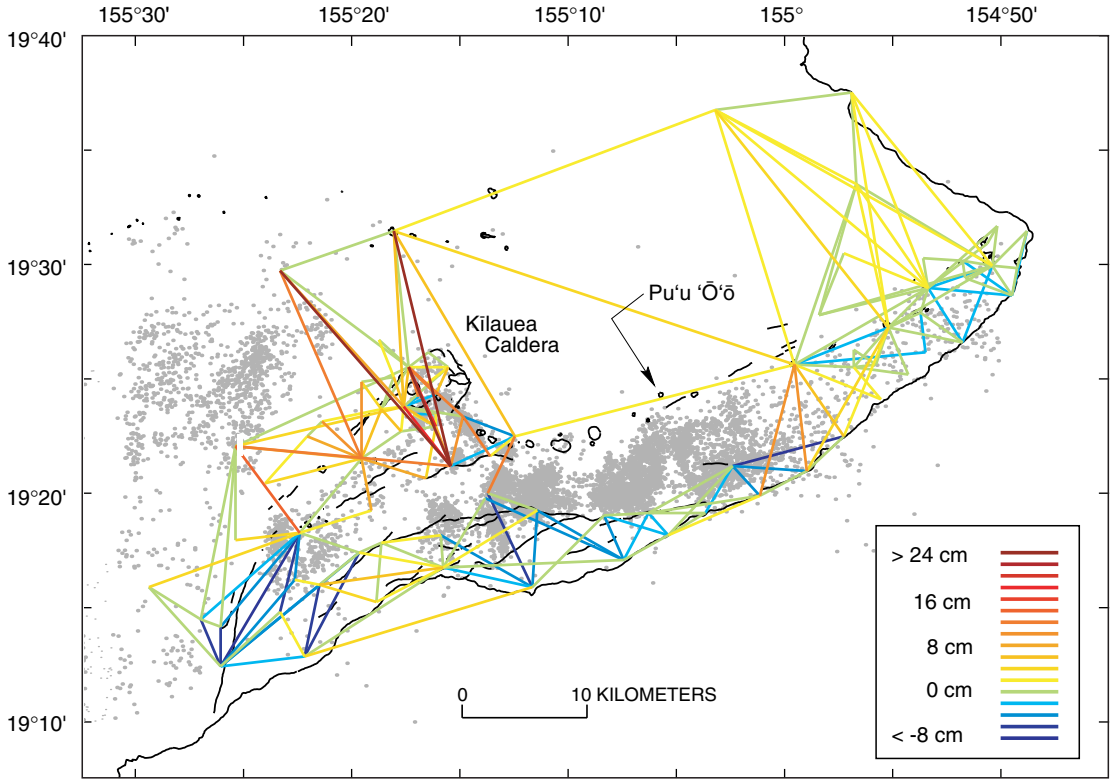

Figure 2. Map of Kīlauea showing rates of relative displacements (in centimeters per year) recorded by trilateration between 1976 and 1982. Positive values are extension; negative values are shortening. Trilateration measurements are estimated to have a fixed error of 1 cm and a scale error of 1 ppm (Delaney and others, 1994, table C-1).

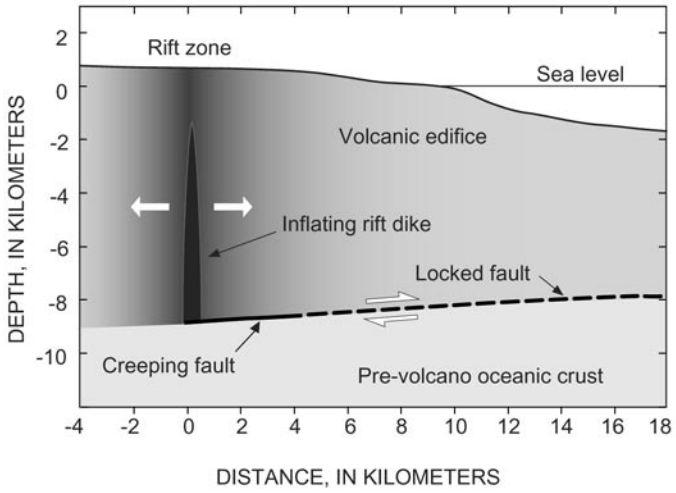

Figure 3. Schematic cross section across the east rift zone of Kīlauea showing principal structural elements used in modeling deformation data. Overpressure in dike drives flank deformation. Dashed line indicates locked portion of the basal fault.

quantitative comparisons between the stresses obtained from modeling the deformation data with stresses obtained from seismicity. The method is summarized here.

This method builds on the widespread demonstration that changes of stress correlate with changes of earthquake-activity rates (Simpson and Reasenberg, 1994; King and others, 1994; Jaumé and Sykes, 1996; Harris and others, 1995; Stein, 1999). Specifically, earthquake rates tend to increase (or decrease) in regions where the Coulomb failure stress function increases (or decreases). Coulomb stress S is defined as

$$S = \tau - \mu\sigma, \qquad (1)$$

where τ is the shear stress acting across fault planes that generate earthquakes (positive in the slip direction), σ is the normal stress (less pore fluid pressure), and μ is the coefficient of fault friction. However, stress changes and earthquake rate changes are not linearly correlated, and earthquake rate changes are strongly time-dependent. Consequently, estimating stress changes from changes of earthquake activity is not straightforward. These nonlinear effects are quite apparent at Kīlauea, where magmatically induced stress changes of a few MPa give rise to swarms of earthquake activity in which earthquake rates may temporarily jump by a factor of 100 or more and then decay with time in the manner of an aftershock sequence, with rates falling by t^{-1} (where t is time following the stress change).

To account for these nonlinear effects, changes of Coulomb stress are determined from changes of earthquake rates using a formulation (Dieterich, 1994) derived from laboratory observations of rate- and state-dependence of fault friction. This formulation includes the non-linear dependence of earthquake rates on stress and provides a physical model for aftershocks including the time-dependence of the Omori aftershock decay law. Earthquake rate R (in a specified magnitude range) is

$$R = \frac{r}{\gamma \dot{S}_r}, \text{ where } d\gamma = \frac{1}{A\sigma}[dt - \gamma dS] \qquad (2)$$

and where γ is a state variable, t is time, and S is a Coulomb stress function in which the friction term in equation (1) is defined as $\mu=\tau/\sigma-a$. The constant r is defined as the steady-state earthquake rate within the selected volume, at the reference stressing rate $\dot{S}_r$. A is a dimensionless fault constitutive parameter with values, measured in laboratory experiments, usually in the range 0.005 to 0.015 (Dieterich, 1994; Dieterich and Kilgore, 1996; Scholz, 1998). We assume μ=0.35 in computing Coulomb stresses from the deformation model to compare with the seismicity stress solutions. This value is based on an assumed sliding friction (τ/σ) of 0.6, which is reduced by the parameter a, estimated as 0.25 from laboratory studies (Linker and Dieterich, 1992; Dieterich, 1994).

To determine stress changes in some volume, the observed seismicity rate as a function of time $R(t)$ is used to directly calculate γ as a function of time (that is, from equation 2, $\gamma(t)=r/R(t)\dot{S}_r$). Using a time-marching procedure, the differential equation 2 is then solved for the Coulomb stress as a function of time. Dieterich and others (2000) provide additional information. The earthquake rates are smoothed before solving for S to reduce noise in the solution, which arises from the random component of earthquake occurrence. This procedure gives the change of Coulomb stress that is driving the earthquake process. On average, we assume earthquakes occur on faults that are optimally oriented in the stress field. The stress field may not have a constant orientation across the region and may change orientation with time. The procedure, as currently implemented, does not provide information on stress orientation.

The calculation for γ requires estimates of r and $\dot{S}_r$; r is taken to be the average earthquake rate in the volume over the entire time interval from January 1976 to January 2000. The calculations are performed in terms of the normalized Coulomb stress ($S/A\sigma$), which permits the parameter $\dot{S}_r$ to be replaced by the observable quantity t_a, the aftershock duration. From Dieterich (1994),

$$t_a = A\sigma/\dot{S}_r \qquad (3)$$

and is defined as the characteristic time for seismicity rates to return to the background rate r. Finally, the scaling of results to stress in MPa requires the additional estimation of the term $A\sigma$. Comparisons between the normalized Coulomb stresses and results of deformation modeling indicate $A\sigma$ has values in the range 0.25 to 0.45 MPa. For this study all results have been scaled using $A\sigma$=0.30MPa.

Maps of Coulomb stress change over specified time intervals were derived by repeating these calculations at nodes in a grid superimposed over Kīlauea. The grid has a regular node spacing of 1 km in both the x and y directions. Seismicity rates were obtained within cylindrical volumes, between hypocentral depths of 6 and 13 km, centered on each node. Within each volume, with a starting radius of $\sqrt{0.5}$ km, we required a minimum average seismicity rate of eight events per year, M≥1.5. If the seismicity within the initial volume did not meet this criterion, the search radius about that node was increased in increments of $\sqrt{0.5}$ km until the minimum average rate of eight events per year was obtained or the maximum search radius of $4\sqrt{0.5}$ km=2.83 km was exceeded. At 2.83 km, if

the corresponding volume did not produce at least eight earthquakes per year, Coulomb stress change was not computed. Using these procedures, we mapped Coulomb stress changes for most of Kīlauea's south flank. A similar procedure was used to obtain stress solutions for selected cross sections.

Figure 4 shows examples of calculations at representative nodes in the study area. The eight-per-year criterion used for these solutions, together with randomness in earthquake times, results in somewhat noisy solutions. However, the noise due to earthquake randomness is not spatially coherent, while changes due to underlying stress changes have spatial coherence. The eight-per-year criterion provides a reasonable balance between optimizing for spatial resolution and enhancing signal to noise at each node.

Results

Deformation and Stress Changes, 1976 to 1983

This time interval consists of the period following the 1975 Kalapana earthquake and before the onset of the Pu'u 'Ō'ō-Kūpaianaha eruption. The spatial and temporal resolution of the deformation data for this interval precludes detailed modeling of local events and small-scale structures. Consequently, the deformation models seek principally to represent the overall deformation of the volcano, and they assume that both the sporadic shallow dike intrusions and the steady magma reservoir can be modeled as the cumulative deformation of a single dike.

During the period from 1976 to 1983, trilateration baselines (fig. 2) show rapid horizontal extension across the caldera and rift zones. This extension is particularly fast in the upper parts of the rift zones, and the maximum extension of as much as 26 cm/yr occurs across the summit caldera. Most of the baselines that span the south flank, particularly those perpendicular to the rift zones, experienced compression of as much as 9 cm/yr. The flank compression during this period differs from measurements after 1983, which show flank extension (Delaney and others, 1998; Owen and others, 1995). Negligible deformation rates are recorded in the easternmost part of the rift system, as well as on the north flank of the volcano. Subsidence along the rift-system axis (up to 7 cm/yr) and uplift of the south flank (up to 2.5 cm/yr) accompany the large horizontal displacements (fig. 5). This uplift is confirmed by data from tide gauges and water-well level data (table 1).

On the basis of deformation modeling, the depth of the top of the rift-zone dike, its dip, and the area of fault creep are reasonably well constrained by the trilateration observations. For a fault depth of 9 km, our preferred model (fig. 6) gives the best fit to the trilateration data (smallest χ^2 error on relative displacements) with a vertical dike 8.5 km high, dilating at an average rate of 40 cm/yr, and coupled slip on a fault dipping 5° to the northwest. The low-angle fault creeps passively (constant stress) over the narrow aseismic area south

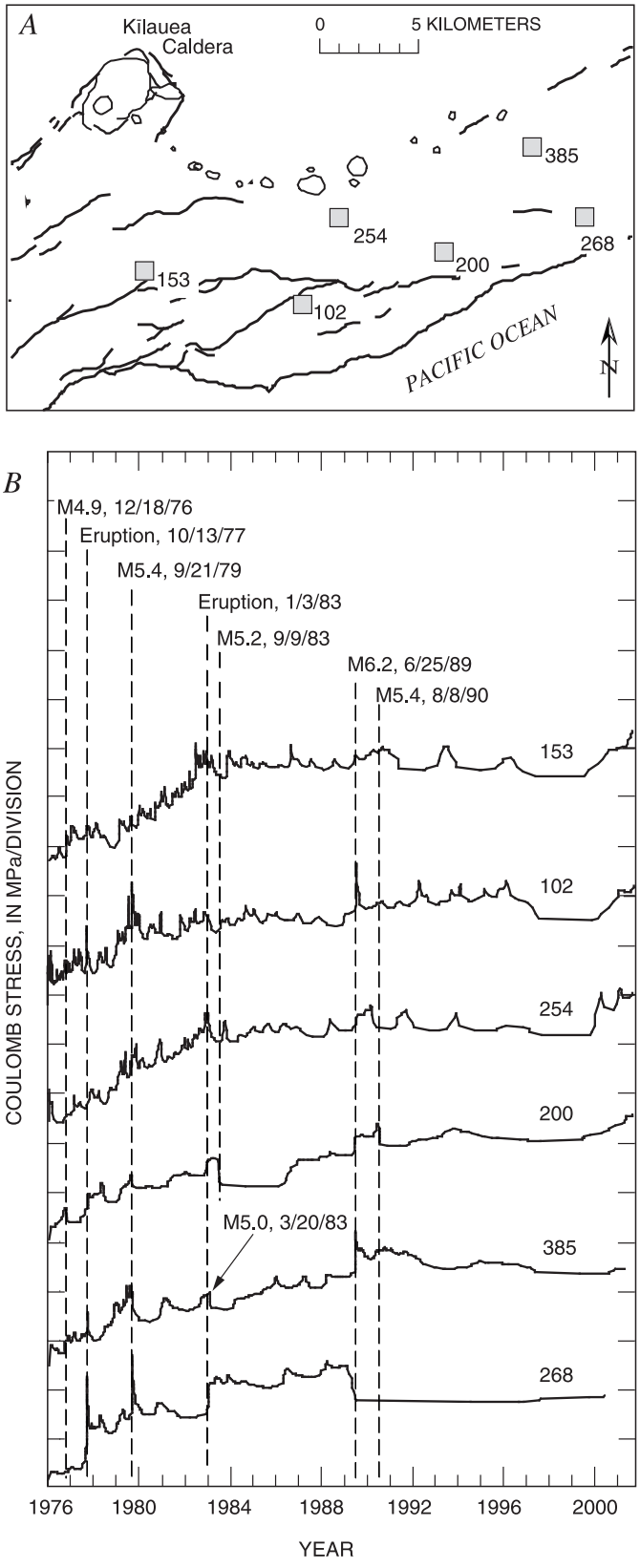

Figure 4. *A*, Index map of study region for solution of Coulomb stress changes from seismicity rate changes. Numbered symbols indicate locations of selected records of stress vs. time given in *B*. *B*, Representative solutions for Coulomb stress vs. time solutions. Vertical dashed lines indicate times of earthquakes and east-rift-zone eruption onsets.

of the rift zone. At the ground surface, this model results in an average rift-zone opening of 20 cm/yr. This model also gives the best fit of the leveling data (fig. 5). However, the sharp subsidence along line b–b′ (fig. 5) associated with the August 1981 southwest rift intrusion cannot be resolved by the elastic modeling (Pollard and others, 1983). Modeled height changes are also comparable to those obtained from sea-level measurements (table 1).

Table 1. Comparison between measured and predicted elevation changes at water wells and tide gauge for 1976–82.

[Water well and Āpua tide gauge data (Āpua tide) are derived from the interpolations given by Delaney and others (1998).]

Location	Latitude and Longitude	Elevation (cm/year)	
		Measured	Modeled
Kapoho	19°30', 154°50'	-1.4±0.7	0.2
Mālama Ki	19°27', 154°53'	-1.7±0.6	0.7
Pūlama	19°21', 155°20'	5.0±1.2	7.0
ʻĀpua tide	19°16', 155°12'	5.7±1.3	6.0

Models with dike dilation but no fault slip fit the trilateration data, but they lead to an underestimation (as much as 50 percent) of rift-zone subsidence (line a–a′). Compared to the best-fit solution, in which the fault is allowed to slip over a larger uniform width of 10 km, the error (χ^2) on distance variation increases by 10 percent, south flank compression is not accounted for, and the rift zone subsidence is overestimated by as much as 40 percent. The overestimation of the south flank uplift remains the same when the fault is horizontal. Trilateration data give little constraint on the fault depths and dike height nor on the precise western and eastern extent of the dike. Indeed, trilateration data are equally well explained by a fault located in the depth range 6 to 11 km and for a rift system 4 km shorter or longer to the west or to the east.

The total calculated Coulomb stress change in the preferred model along a cross section that includes the location of the January 1983 eruptive fissures is shown in figure 7*A*. For calculation of Coulomb stress in the deformation model, we assume μ=0.35 and resolve stress changes on fault planes parallel to the decollement with a sense of slip such that the upper block moves away from the rift zone. Projected onto this cross section are earthquakes from the start of 1980 to the start of 1983, as well as the M7.2 earthquake of 1975 and the M6.2 earthquake of 1989. Note the good correspondence between earthquake activity and the region of high Coulomb stress.

Coulomb stress changes have been determined from earthquake rate changes along the cross section of figure 7*A*. At this location, the seismicity stress solution over the 1976 to 1983 interval (fig. 7*B*) may not be equivalent to the regional deformation model, because significant local stressing events altered the local stress conditions in this area but are not resolvable in the deformation data. These local events are discussed below and include the dike intrusion and eruption of September 1977 and several earthquakes in the magnitude range 4.6 to 5.4. Consequently, we believe the stress change calculated for the interval from 1980 to 1983 (fig. 7*C*), which lacks eruptive events or significant earthquakes, is probably a more appropriate comparison with the deformation model. The seismicity stress solution for 1980 to 1983 agrees with the deformation model in the overall pattern of stress changes, including the region of maximum stress increase adjacent to the end of the zone of inferred fault creep. However, the average maximum stress change is about 0.6 MPa/yr (1976–83) in the

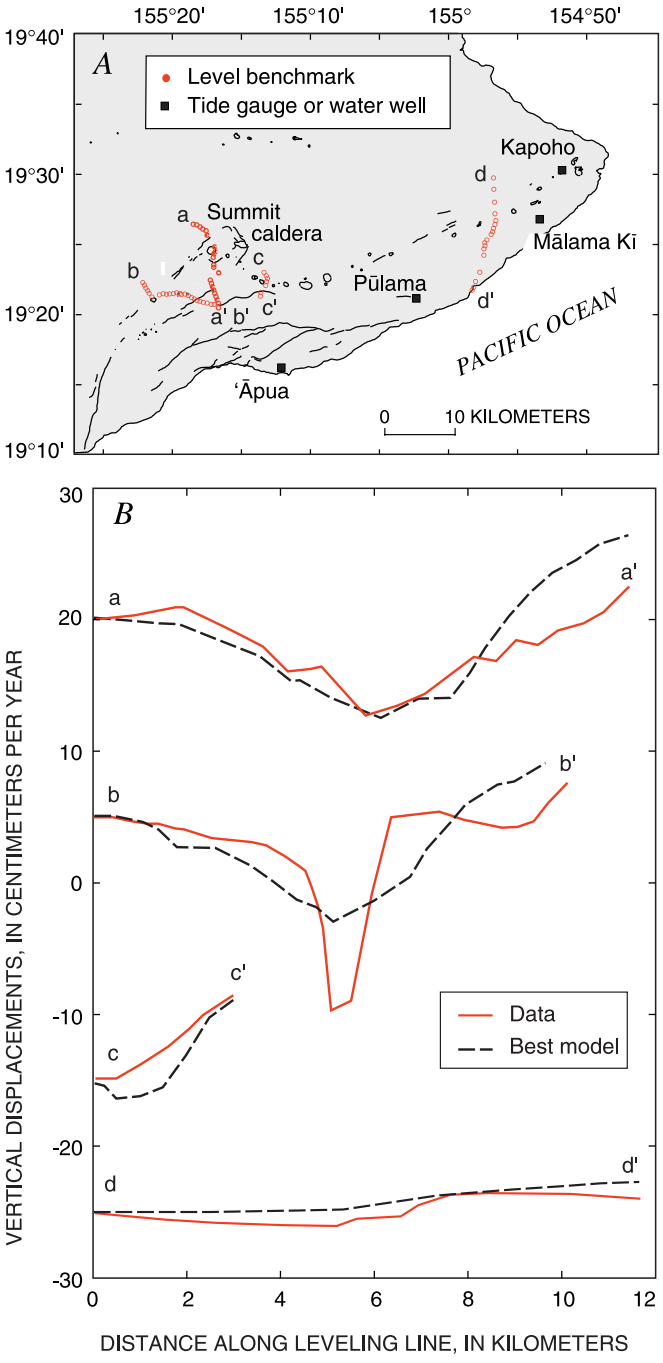

Figure 5. *A*, Location of leveling lines, tide gauge, and water wells used in deformation modeling of Kīlauea Volcano for the period from 1976 to 1983. *B*, Comparison of relative vertical velocities measured (red lines) and predicted by best-fitting model (black lines) along four lines shown in *A*.

deformation model compared to about 0.2 MPa/yr (1980–83) for the seismicity solution. Below we show that this difference is consistent with a regional slowing of stressing rates that occurred in this area around the start of 1980.

The pattern of stress change from the seismicity solution (fig. 7*C*) provides added support for the preferred deformation model. This model, with a narrow zone of fault slip, differs substantially from those obtained for 1983–91 by Delaney and others (1993) and for 1990–93 by Owen and others (1995). Coulomb stresses in models with much wider zones of fault creep, as employed by Delaney and others (1993) to model the 1983–91 period and by Owen and others (1995) to model the 1990–93 period, appear to be inconsistent with the earthquake data. Indeed, models lacking a zone of fault creep, or with a wider zone of fault creep than used here, place the greatest stress change in regions devoid of earthquakes and have low stress in the area of earthquake activity.

The Eruptions of 1983 and 1977

The Pu‘u ‘Ō‘ō-Kūpaianaha eruption was initiated by a shallow intrusion that opened the rift zone by about 2 m (Dvorak and others, 1986; Okamura and others, 1988; Hall Wallace and Delaney, 1995) and, on January 3, 1983, reached the surface to form a line of eruptive fissures (fig. 8 *A*, *B*, *C*). The boundary element models for Coulomb stress change for the onset of the 1983 eruption are based on horizontal displacements from trilateration measurements and on dry tilt data. We have computed deformation and stress changes for a model in which the inferred deep, pre-existing, inflating rift dike propagates from a depth of 3 km to the free surface, and for a model of an isolated intrusion of a shallow dike (Okamura and others, 1988; Hall Wallace and Delaney, 1995) in which the deeper dike and fault are not involved. Both models fit the deformation data equally well and have a dike opening at the surface of 2.1 m.

Several factors lead us to strongly favor the deep-dike model (fig. 8*B*) over the shallow-dike model (fig. 8*A*). First, it is a mechanically consistent extension of the preferred model for the 1976–83 period. Second, the pressure required to open the shallow dike in the preferred model is internally consistent with that model—the dike opens in response to a stress increase equivalent to the increased pressure required to lift magma the 3 km to the surface. The pressure in the shallow-dike model was adjusted to give the best fit to the data and is nearly twice that in the deep-dike model. The large pressure increase required for the shallow-dike model appears difficult to justify on physical grounds. Third, the preferred model agrees with both earthquake locations and seismicity stress solutions (fig. 8*C*), while the shallow-dike model agrees with neither. At the time of the intrusion, seismicity rates in this region of the south flank immediately increased by as much as a factor of 100. Relative to the pre-intrusion period, activity shifted away from the rift zone, and more shallow events occurred in regions of increased stress (compare figure 7*A* with figure 8*B*). Stress changes obtained from the seismicity (fig. 8*C*) are in good agreement with the stress-change calculations in the preferred model of a deep pre-existing dike (fig. 8*B*). In particular, in the depth range of 6 to 10 km (fig. 8 maps), the preferred deformation model and the seismicity solution (fig. 8*C*) show a region adjacent to the rift zone that undergoes a modest stress decrease. This pattern arises in the preferred deformation model specifically because the basal fault adjacent to the rift zone is allowed to slip in response to the intrusion and to increased pressure in the pre-existing rift dike. Farther away from the rift is a region of large stress increase that originates from the combined effect of the shallow rift expansion and the

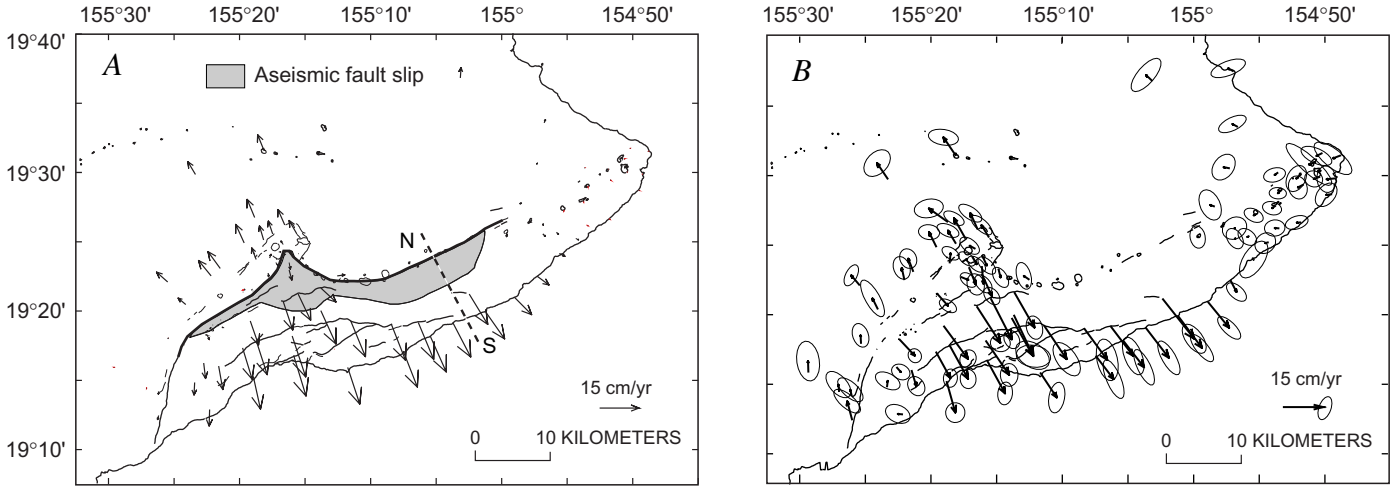

Figure 6. *A*, Horizontal velocities at ground surface of Kīlauea Volcano predicted by best-fit model for the period from 1976 to 1983. Location of model dike is indicated by bold line. Creeping portion of low-angle fault at base of the volcano is indicated by gray. The remainder of the fault is locked. Dashed line indicates location of cross sections in figure 7. *B*, Measured velocities determined from model coordinate network adjustment (Segall and Matthews, 1988) performed with reference to velocity model given in *A*. Ellipses are 95-percent confidence interval.

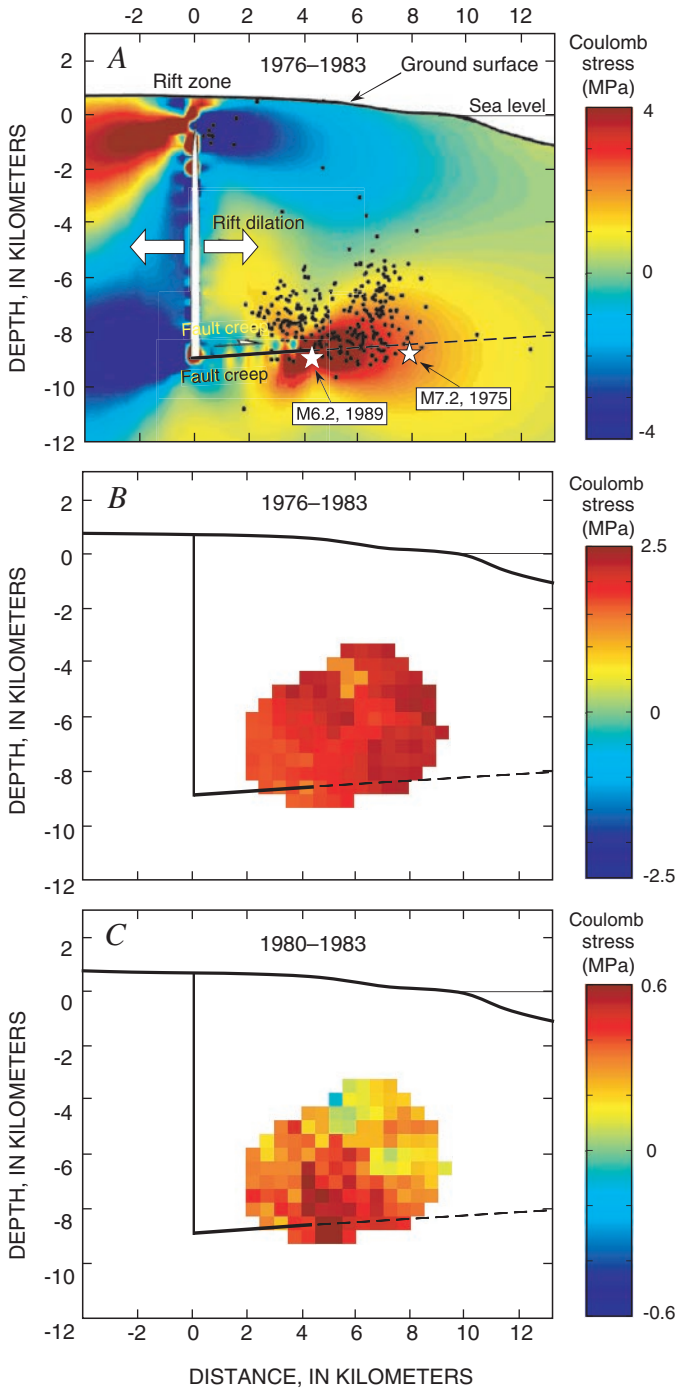

Figure 7. Coulomb stress changes prior to onset of Pu‘u ‘Ō‘ō-Kūpaianaha eruption of January 3, 1983, shown on cross sections of south flank and east rift zone through zone of Pu‘u ‘Ō‘ō-Kūpaianaha eruptive fissures. See figure 8 for location of cross section. *A*, Coulomb stress changes from preferred deformation model for the period from 1976 to 1983 and earthquakes (M≥1.5) (shown as dots and stars) for the period from 1980 to 1983. Coulomb stress computation assumes failure planes parallel to basal fault such that positive Coulomb stress promotes seaward (SSE) motion of upper block. *B*, Seismicity stress solution for the period from 1976.0 to 1982.9 (using decimal notation for parts of years). *C*, Seismicity stress solution for the period from 1980.0 to 1983.0.

deep fault slip. In contrast, the stress changes derived from the shallow-dike model (fig. 8*A*) bear little resemblance to stresses from the seismicity solution. Also, the region of high stress increase north of the rift zone, in the depth range of 6 to 10 km (fig. 8*A*), is devoid of earthquake activity.

Previously, Cayol and others (2000) presented a quantitative comparison of results for the cross-sectional stresses resulting from the 1983 intrusion (but using a somewhat different approach to solving equation 2 with stresses from this boundary element model). Regression of the Coulomb stresses from the boundary element model of the intrusion against stresses from the seismicity calculation yielded a slope of 1.1 and a correlation coefficient of 0.80.

The preferred deformation model of the 1983 intrusion also appears to be a reasonable representation of the stress changes for the September 1977 intrusion and eruption. Each intrusion occurred in the same region, and the limited deformation data for the 1977 event are consistent with the more extensive 1983 data set. Significantly, each resulted in similar changes in seismicity patterns and rates. Consequently, the resulting seismicity stress solution for the 1977 intrusion (fig. 8*D*) is very similar to the 1983 solutions. The principal difference appears to be a somewhat larger magnitude of stress increases in 1977. This is consistent with measurements made of geodimeter lines (Pūlama-Kupapa‘u and Queen’s Bath-Ford), which suggest much larger flank compression at the time of the 1977 intrusion compared to the 1983 intrusion (Arnold Okamura, oral commun., 2002).

Flank Earthquakes

In addition to the magmatic deformation sources in the east rift zone, the adjacent region of the south flank is also subjected to internal stressing from earthquakes. Since 1976, significant earthquakes in this area include the 1989 M6.1 Kalapana earthquake and several moderate earthquakes in the range M4.7 to M5.4 (fig. 9). The somewhat limited deformation data related to the 1989 Kalapana earthquake have been analyzed by Arnadottír and others (1991), who determined that the best-fitting dislocation source was a gently dipping thrust fault extending east of the hypocenter, into a region of low seismicity. The M4.9–M5.4 earthquakes, which are typically at depths of 7 to 10 km, are generally too small and too deep to result in diagnostic surface deformations adequate for modeling purposes. However, such events are expected to significantly alter stress conditions on length scales on the order of one or two source dimensions (that is, 5 to 10 km) by amounts comparable to those of larger earthquakes, because earthquake stress drops are independent of magnitude. This is apparent in the seismicity stress solutions for these moderate flank earthquakes (fig. 9).

Detailed comparisons of these solutions with models based on deformation observations are not possible, but it is instructive to compare them to a generalized boundary element model of a moderate earthquake (fig. 10*A*). The model represents an earthquake of about M5.0 and consists of a

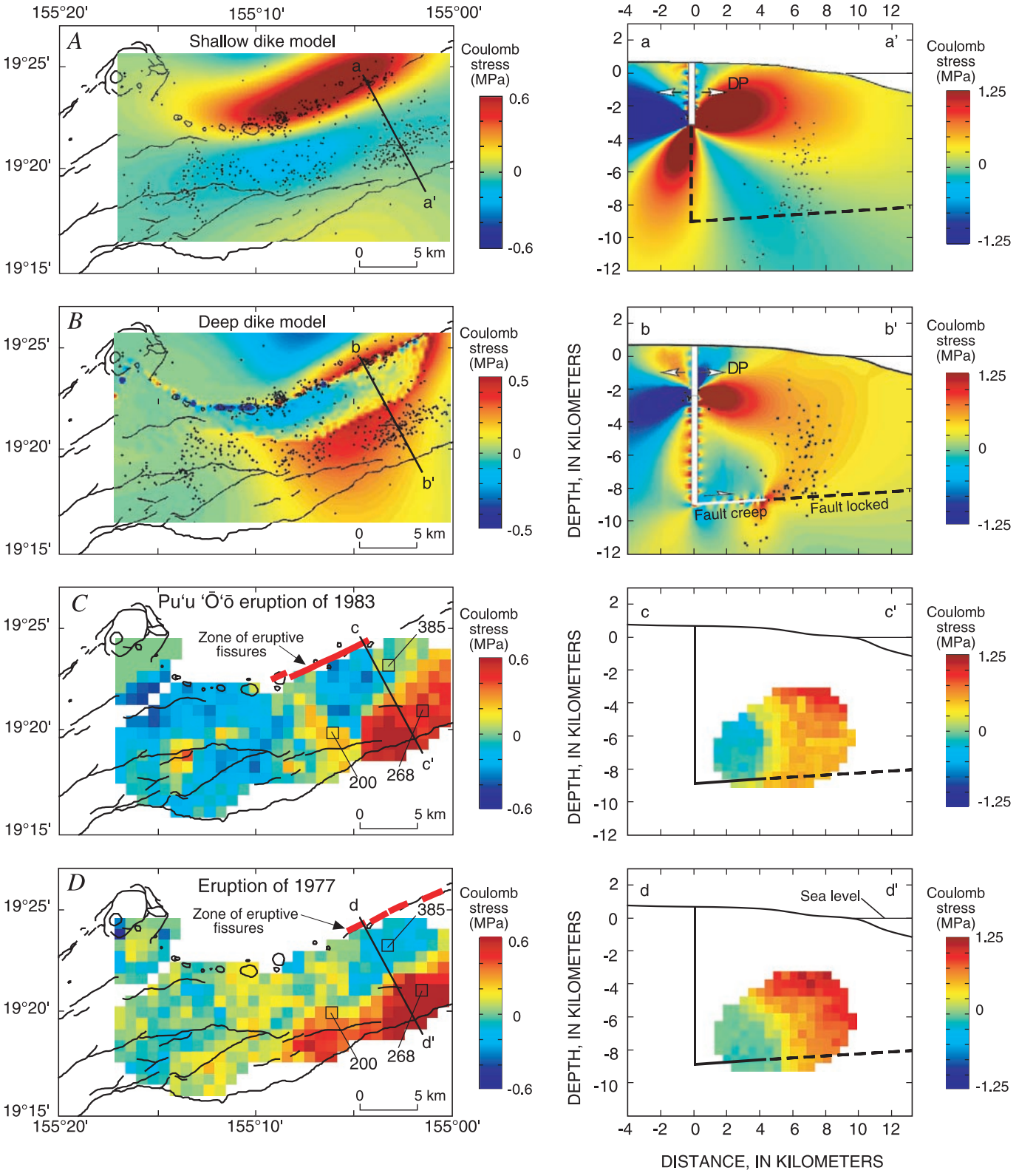

Figure 8. Coulomb stress changes at time of September 13, 1977, and January 3, 1983, east rift eruptions. *A*, Map and cross section of Coulomb stress changes computed from deformation model of onset of 1983 Pu‘u ‘Ō‘ō-Kūpaianaha eruption using shallow-dike model. Earthquakes shown (as dots) are M≥1.5 for 90 days following the onset of Pu‘u ‘Ō‘ō-Kūpaianaha eruption. *B*, Map and cross section of Coulomb stress changes computed from deformation model of onset of 1983 Pu‘u ‘Ō‘ō-Kūpaianaha eruption using preferred deep-dike model. Earthquakes shown as in *A*. *C*, Coulomb stress changes from seismicity rate changes at onset of the Pu‘u ‘Ō‘ō-Kūpaianaha eruption. See figure 4 for records of stress vs. time for the indicated nodes. *D*, Coulomb stress changes from seismicity rate changes at the onset of the September 1977 eruption.

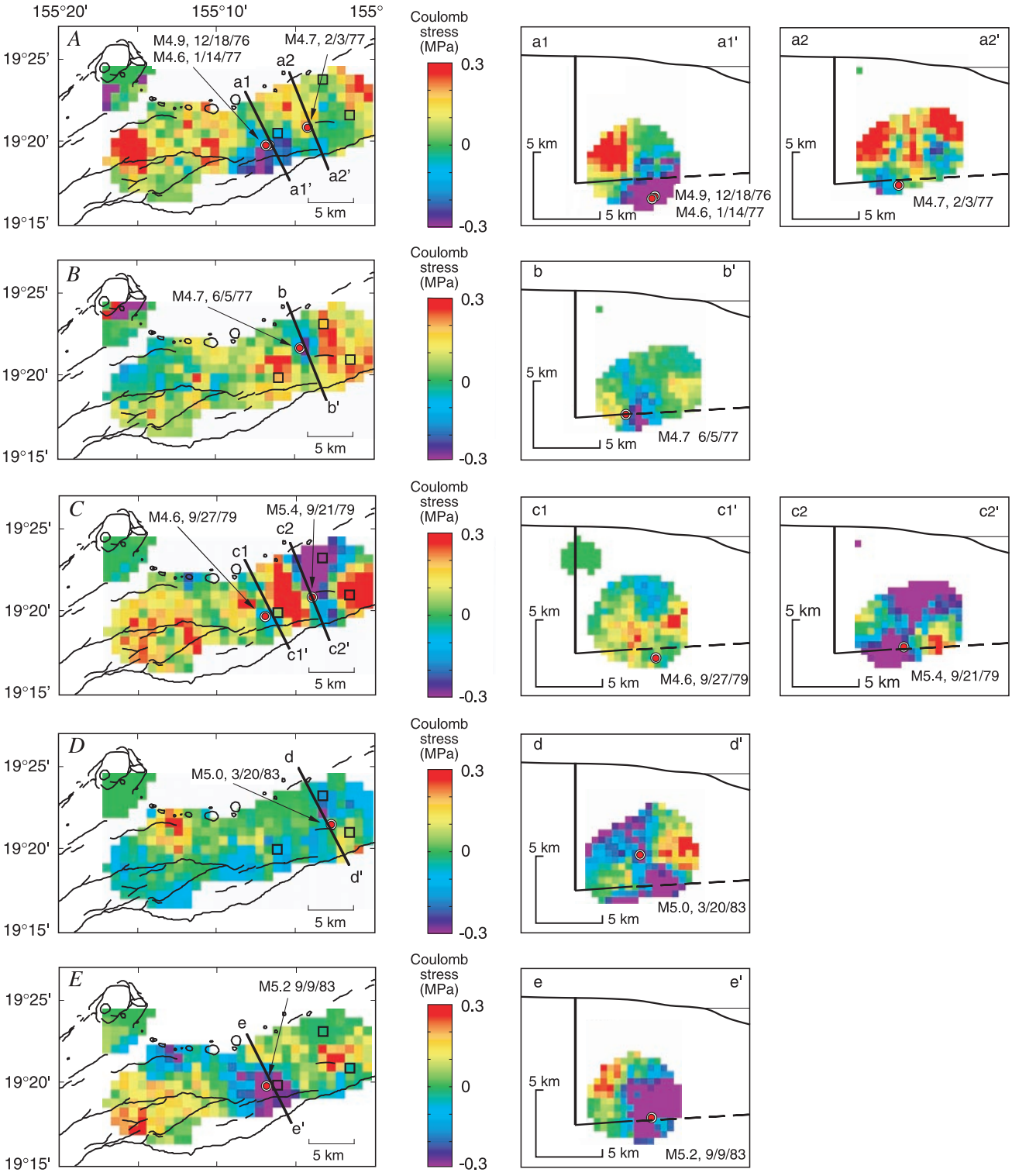

Figure 9. Coulomb stress changes computed from seismicity rate changes for earthquakes M≥4.7 in vicinity of Pu‘u ‘Ō‘ō-Kūpaianaha eruption. Small squares on map view indicate locations of records of stress vs. time in figure 4.

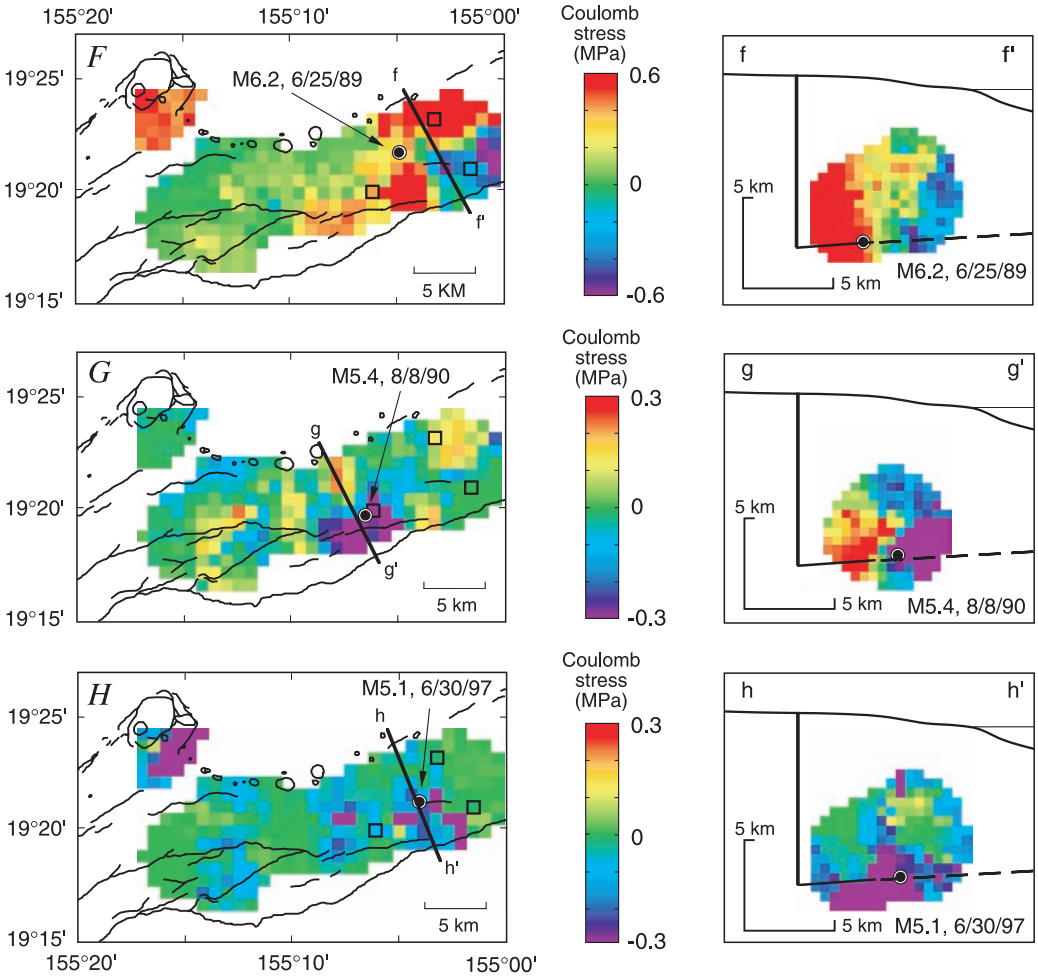

Figure 9. Continued.

horizontal circular rupture source 5 km in diameter and a uniform stress drop of 1 MPa. To facilitate comparisons with the seismicity solutions, which use earthquakes principally in the depth range of 6 to 10 km, the Coulomb stresses have been averaged over a depth interval of ±2 km centered on the fault plane. Figure 10*B* shows a simulated seismicity stress solution based on the boundary element model. In this simulation, earthquake rates as a function of time and position were first calculated from the stress changes of the boundary element model using equation 2. Next, using the predicted rates, earthquake event times were randomly drawn to produce a synthetic earthquake catalog. The unperturbed earthquake rates of the synthetic catalog (r in equation 2) were chosen to be representative of the south flank rates. Finally, the synthetic catalog was used to solve for the stress changes using the procedures employed for the real data (fig. 10*B*). The simulation indicates that sources 5 km in diameter, or somewhat smaller, should be resolvable using the seismicity solution method.

In map view, the solutions for stress changes at the time of earthquakes of M≥4.7 give regions of stress decrease near the earthquake hypocenter and stress increase in adjacent regions. These patterns are in general agreement with the model earthquake. Most prominent in these solutions are the regions of stress decrease, or "stress shadows," where seismic activity slowed following the earthquake. The dimensions of the regions of stress decrease are typically 4 to 8 km, consistent with fault slip lengths expected for earthquakes of these magnitudes.

In cross section, the Coulomb stress solutions of four earthquakes (M4.7, 6/5/77; M4.6, 9/27/79; M5.4 9/21/79; M5.0, 3/20/83) in figure 9*B*, *C*, and *D* show the characteristic pattern of stress decrease and increase expected for slip on a fault patch. That pattern has a region of stress drop between two zones of stress increase, presumably marking the region of fault slip and regions of stress concentration at the ends of the slip zone, respectively. Four other events (M4.9, 12/18/76; M5.2, 9/9/83; M6.2, 6/25/89; M5.4, 8/8/90) in figure 9*A*, *E*, *F*, and *G* appear to have incomplete patterns of stress change consisting of a single region of stress increase adjacent to the region of stress decrease. The earthquakes with these patterns are, on average, larger than those events showing the more complete pattern, and all lie at the edge of the region where seismicity stress solutions are possible according to our

criteria. Consequently, we interpret these cross sections to represent sources that lie partly outside the solution region. Two earthquakes (M4.7, 2/3/77; M5.1, 6/30/97) in figure 9*A* and *H* have complicated patterns that may represent complex, multi-segment events or sources that are misoriented with respect to the cross sections.

South flank earthquakes, especially the larger events, relieve rift expansion stresses and thereby permit continued expansion of the rifts and the accompanying intrusion of magma into the rifts (Dieterich, 1988). The intrusion and eruption of September 13, 1977, were preceded by the M4.7 earthquake of June 5, 1977, and followed by the M5.4 earthquake of September 2, 1979 (figs. 9*B* and 9*C*, respectively). The 1979 event, in particular, relieved the 1977 intrusion stresses and may have permitted movement of magma into the portion of the rift zone that resulted in the eruption of Pu‘u ‘Ō‘ō-Kūpaianaha on January 3, 1983.

Following the onset of the Pu‘u ‘Ō‘ō-Kūpaianaha eruption, most larger earthquakes initiated within the region of stress increase that developed at the time of the 1983 intrusion and eruption (fig. 7). The single exception is the M6.2 1989 earthquake, which initiated outside that zone of stress increase. However, the region of maximum stress drop for that earthquake did coincide with this region of maximum stress increase (compare figure 8*B* with figure 9*F*). This is also evident in the stress/time record of node 268 (fig. 4), which clearly shows the stress increases at the times of the 1977 and 1983 eruptions and the stress decrease at the time of the 1989 earthquake.

In the vicinity of node 200, there were repeated moderate earthquakes of M4.9, M4.6, M5.2 and M5.4 on 12/18/76, 9/2/79, 9/9/83, and 8/8/90, respectively (figs. 4 and 9*A*, *C*, *E,* and *G*). These events are evident as stress drops at node 200 (fig. 4). In addition, this location experienced stress increases at the times of the 1977 and 1983 intrusions as well as the 1989 earthquake. This record gives an impression of recurring fault failure at a threshold stress.

Stressing Rate Changes in 1979 and 1983

Comparison of the trilateration line length changes in the 1976–82 period with those after 1983 shows widespread slowing of deformation rates sometime around the time that the Pu‘u ‘Ō‘ō-Kūpaianaha eruption began. Extension rates across Kīlauea caldera averaged about 25 cm/yr in the years leading up to the Pu‘u ‘Ō‘ō-Kūpaianaha eruption and decreased to about 4 cm/yr at the onset of the eruption (Delaney and others, 1998), a slowing by a factor of about five. Across the east rift zone, a similar slowing of rates of extension occurred, and south-flank lines oriented perpendicular to the rift zone changed from compression to extension (Delaney and others, 1998). South of the east rift zone, a slowing of stressing rates is very evident in the seismicity solutions. For much of the region, the stress versus time data (fig. 4) indicate average stressing rates of about 0.25±0.10 MPa/yr in the 1976–80 period and about 0.05±0.02 MPa/yr after 1983, roughly a factor of five decrease that is consistent with the deformation data. This slowing occurred quite abruptly around the end of 1979 in some regions (fig. 4, nodes 102, 385, and 268) and at the start of 1983 in other areas (fig. 4, nodes 153, 254, and possibly 200).

Regions affected by a change of stressing rates near the end of 1979 are shown in figure 11*A*, which plots the average stressing rate in the interval from 1980.0 to 1982.5 (the exact temporal midpoint of the year 1982) minus the average

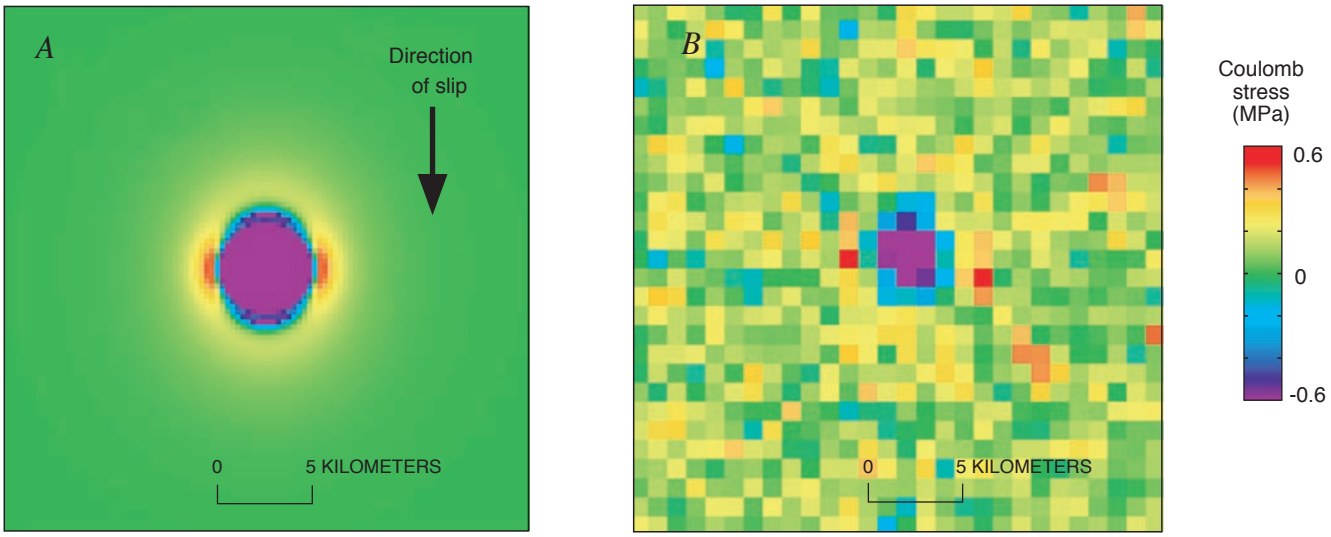

Figure 10. Generalized model of M~5 earthquake. View is perpendicular to fault plane. *A*, Boundary element model of slip in which stresses have been averaged over a width of ±2 km of the fault surface. *B*, Solution for stress changes from simulated earthquake catalog derived from boundary element model of *A*, together with earthquake rate formulation given by equation 2.

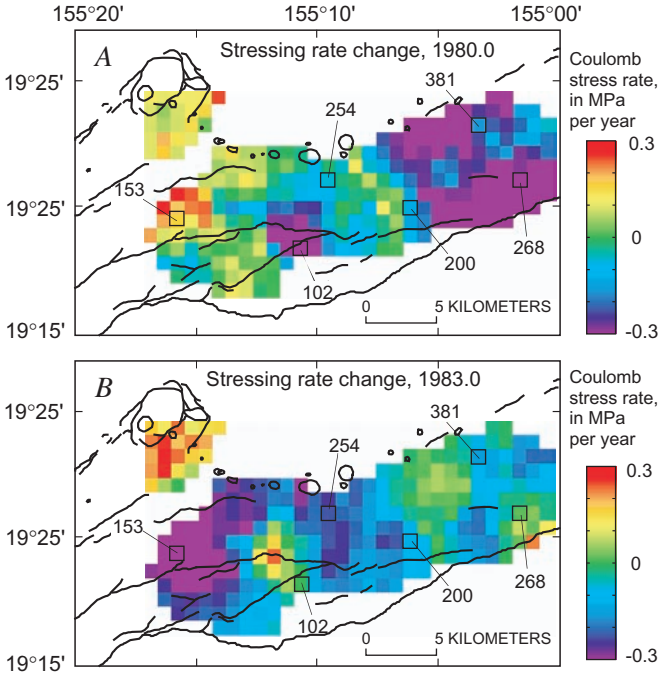

Figure 11. Change of Coulomb stressing rates. Plots give change of stressing rate $\Delta\dot{S}_r=\dot{S}_2-\dot{S}_1$, where $\dot{S}_1$ and $\dot{S}_2$ are average Coulomb stressing rates in successive time intervals 1 and 2, respectively. Numbered squares indicate the locations of the records of time vs. stress in figure 4. *A*, Change of stressing rate near the start of 1980 using average stressing rates in time intervals 1976.0–1980.0 and 1980.0–1982.5 (using decimal notation for parts of years). *B*, Change of stressing rate at start of 1983, using average stressing rates in time intervals 1980.0–1983.0 and 1983.0–1988.5.

stressing rate in the interval from 1976.0 to 1980.0 from the seismicity stress solutions. The region most affected by this slowing coincides quite closely with the area affected by the M5.4 earthquake of 9/21/79 (fig. 9). In addition, the stressing rate of an isolated region to the west (in the area of node 102) also slowed dramatically. Figure 11*B* shows regions affected by slowing at the start of 1983.

The slowing of flank stressing at the start of 1983 indicates that the volume of lava for the Pu‘u ‘Ō‘ō-Kūpaianaha eruption represents a major fraction of the magma supplied to Kīlauea. On the basis of rift-zone volume change in the preferred deformation model for the 1976–83 period, the rate of supply of magma to the rift zones has been modeled to be 0.18 km^3/yr (Cayol and others, 2000). Wolfe and others (1987) estimated an average eruption rate of 0.12 km^3/yr from February 1983 to June 1984, and Heliker and Mattox (this volume) obtained a rate of 0.12 km^3/yr over the first 19 years of the eruption. Assuming a constant supply rate of 0.18 km^3/yr and eruptive rates of 0.12 km^3/yr, the volume of magma available to drive rift expansion decreased from 0.18 km^3/year to 0.06 km^3/yr after the onset of the eruption. Within the uncertainties of these estimates, this inferred three-fold reduction of magma to drive rift expansion at the start of the Pu‘u ‘Ō‘ō-Kūpaianaha eruption is reasonably consistent with the five-fold reduction of deformation and stressing rates noted previously.

The cause for the slowing of deformation rates in the eastern portion of the study area around the time of the 1979 earthquake is somewhat problematic. If, as we have argued, deformation of the south flank is driven by movement of magma into the rift system, then the earthquake, which appears to have created a stress condition amenable to continuing intrusion in this area, should have not have resulted in slowing of the deformation. We speculate that the supply of magma to the east rift zone in the area of the Pu‘u ‘Ō‘ō-Kūpaianaha eruptive fissures became temporarily blocked at the time of the earthquake. If this interpretation is correct, then stressing rates in the uprift direction from the blockage (to the west) should have increased around the time of the 1979 earthquake, because the same volume of magma was then driving the deformation over a smaller region. Evidence for this is seen in the weak increase of stressing rates that is evident over much of the western portion of the study area, with a strong increase in stressing rates in the vicinity of node 153, where they increased from about 0.3 MPa/yr to about 0.6 MPa/yr (see the stress vs. time solution for node 153 of figure 4). Additionally, the pattern of slowing at the start of the 1983 eruption (fig. 10*B*) is restricted to the western half of the study area, indicating that magma that was driving the deformation in that region was diverted to feed the 1983 eruption.

Conclusions

An analysis of surface deformation and earthquake data has been carried out for Kīlauea Volcano as it pertains to stress interactions before and during the Pu‘u ‘Ō‘ō-Kūpaianaha eruption. The seismicity analysis employs a newly developed method to solve for Coulomb stress changes from earthquake rate changes. The period following the M7.2 Kalapana earthquake in 1975 and before the start of the Pu‘u ‘Ō‘ō-Kūpaianaha eruption in 1983 was characterized by the rapid expansion of a dike-like magma body within the rift zones of Kīlauea. Both the deformation models and the seismicity stress solutions indicate rift expansion was coupled to aseismic fault slip over a narrow region of a low-angle fault beneath the south flank. The rate of rift opening averaged 40 cm/yr, which is much higher than estimates for any previously analyzed period of Kīlauea deformation. At the onset of the Pu‘u ‘Ō‘ō-Kūpaianaha eruption in January 1983, the inflating rift-zone dike propagated to the surface to form the eruptive fissures. The exceptionally high seismic activity in the south flank adjacent to the east rift zone, and the locations of earthquakes within this zone, are consistent with rapid stressing by an expanding rift zone. In late 1979 and at the start of the Pu‘u ‘Ō‘ō-Kūpaianaha eruption in January 1983, deformation data and seismicity stress solutions indicate a dramatic slowing of deformation and stressing rates in Kīlauea’s south flank. The magnitude of the slowing is roughly consistent with our estimates of magma supply to Kīlauea, based on the deformation modeling of the 1976–83 period.

Acknowledgments

We thank the staff of the Hawaiian Volcano Observatory, particularly Arnold Okamura and Asta Miklius for providing us with the deformation data. Thanks also to Peter Cervelli, Christina Heliker, Ross Stein, and Don Swanson for their thoughtful reviews.

References Cited

Ando, Masataka, 1979, The Hawaii earthquake of November 29, 1975; low dip angle faulting due to forceful injection of magma: Journal of Geophysical Research, v. 84, no. B13, p. 7616–7626.

Árnadóttir, Thóra, Segall, Paul, and Delaney, P.T., 1991, A fault model for the 1989 Kilauea south flank earthquake from levelling and seismic data: Geophysical Research Letters, v. 18, no. 12, p. 2217–2220.

Bryan, C.J., 1992, A possible triggering mechanism for large Hawaiian earthquakes derived from analysis of the 26 June 1989 Kilauea south flank sequence: Seismological Society of America Bulletin, v. 82, no. 6, p. 2368–2390.

Cayol, Valérie, and Cornet, F.H., 1998, Three-dimensional modeling of the 1983–1984 eruption at Piton de la Fournaise Volcano, Réunion Island: Journal of Geophysical Research, v. 103, no. B8, p. 18025–18037.

Cayol, Valérie, Dieterich, J.H., Okamura, A.T., and Miklius, Asta, 2000, High magma storage rates before the 1983 eruption of Kilauea, Hawaii: Science, v. 288, no. 5475, p. 2343–2346.

Cheng, C.H., and Johnston, D.H., 1981, Dynamic and static moduli: Geophysical Research Letters, v. 8, no. 1, p. 39–42.

Clague, D.A., and Denlinger, R.P., 1994, Role of olivine cumulates in destabilizing the flanks of Hawaiian volcanoes: Bulletin of Volcanology, v. 56, no. 6–7, p. 425–434.

Crosson, R.S., and Endo, E.T., 1982, Focal mechanisms and locations of earthquakes in the vicinity of the 1975 Kalapana aftershock zone 1970–1979; implications for tectonics of the south flank of Kilauea Volcano, island of Hawaii: Tectonics, v. 1, no. 6, p. 495–542.

Delaney, P.T., Denlinger, R.P., Lisowski, Michael, Miklius, Asta, Okubo, P.G., Okamura, A.T., and Sako, M.K., 1998, Volcanic spreading at Kilauea, 1976–1996: Journal of Geophysical Research, v. 103, no. B8, p. 18003–18023.

Delaney, P.T., Fiske, R.S., Miklius, Asta, Okamura, A.T., and Sako, M.K., 1990, Deep magma body beneath the summit and rift zones of Kilauea Volcano, Hawaii: Science, v. 247, no. 4948, p. 1311–1316.

Delaney, P.T., Miklius, Asta, Árnadóttir, Thóra, Okamura, A.T., and Sako, M.K., 1993, Motion of Kilauea Volcano during sustained eruption from the Puu Oo and Kupaianaha vents, 1983–1991: Journal of Geophysical Research, v. 98, no. B10, p. 17801–17820.

Delaney, P.T., Miklius, Asta, Árnadóttir, Thóra, Okamura, A.T., and Sako, M.K, 1994, Motion of Kilauea Volcano during sustained eruption from the Puu Oo and Kupaianaha vents, 1983–1991; supplemental information: U.S. Geological Survey Open-File Report 94–567, 23 p.

Dieterich, J.H., 1988, Growth and persistence of Hawaiian volcanic rift zones: Journal of Geophysical Research, v. 93, no. B5, p. 4258–4270.

Dieterich, J.H., 1994, A constitutive law for rate of earthquake production and its applications to earthquake clustering: Journal of Geophysical Research, v. 99, no. B2, p. 2601–2618.

Dieterich, J.H., Cayol, Valérie, and Okubo, P.G., 2000, The use of earthquake rate changes as a stress meter at Kilauea volcano: Nature, v. 408, no. 6811, p. 457–460.

Dieterich, J.H., and Kilgore, B.D., 1996, Implications of fault constitutive properties for earthquake prediction: National Academy of Sciences Proceedings, v. 93, p. 3787–3794.

Dvorak, J.J., Okamura, A.T., English, T.T., Koyanagi, R.Y., Nakata, J.S., Sako, M.K., Tanigawa, W.R., and Yamashita, K.M., 1986, Mechanical response of the south flank of Kilauea volcano, Hawaii, to intrusive events along the rift systems: Tectonophysics, v. 124, no. 3–4, p. 193–209.

Dzurisin, Daniel, Koyanagi, R.Y., and English, T.T., 1984, Magma supply and storage at Kilauea Volcano, Hawaii, 1956–1983: Journal of Volcanology and Geothermal Research, v. 21, no. 3–4, p. 177–206.

Fiske, R.S., and Kinoshita, W.T., 1969, Inflation of Kilauea Volcano prior to its 1967–1968 eruption: Science, v. 165, no. 3891, p. 341–349.

Gillard, Dominique, Rubin, A.M., and Okubo, P.G., 1996, Highly concentrated seismicity caused by deformation of Kilauea's deep magma system: Nature, v. 384, no. 6607, p. 343–346.

Got, J.-L., Fréchet, Julien, and Klein, F.W., 1994, Deep fault plane geometry inferred from multiplet relative relocation beneath the south flank of Kilauea: Journal of Geophysical Research, v. 99, no. B8, p. 15375–15386.

Hall Wallace, M.K., and Delaney, P.T., 1995, Deformation of Kilauea volcano during 1982 and 1983; a transition period: Journal of Geophysical Research, v. 100, no. B5, p. 8201–8219.

Harris, R.A., Simpson, R.W., and Reasenberg, P.A., 1995, Influence of static stress changes on earthquake locations in southern California: Nature, v. 375, no. 6528, p. 221–224.

Hill, D.P., and Zucca, J.J., 1987, Geophysical constraints on the structure of Kilauea and Mauna Loa Volcanoes and some implications for seismomagmatic processes, chap. 37 *of* Decker, R.W., Wright, T.L., and Stauffer, P.H., eds., Volcanism in Hawaii: U.S. Geological Survey Professional Paper 1350, v. 2, p. 903–917.

Jaumé, S.C., and Sykes, L.R., 1996, Evolution of moderate seismicity in the San Francisco Bay region, 1850 to 1993; seismicity changes related to the occurrence of large and great earthquakes: Journal of Geophysical Research, v. 101, no. B1, p. 765–789.

King, G.C.P., Stein, R.S., and Lin, Jian, 1994, Static stress changes and the triggering of earthquakes: Seismological Society of America Bulletin, v. 84, no. 3, p. 935–953.

Klein, F.W., Koyanagi, R.Y., Nakata, J.S., and Tanigawa, W.R., 1987, The seismicity of Kilauea's magma system, chap.

43 *of* Decker, R.W., Wright, T.L., and Stauffer, P.H., eds., Volcanism in Hawaii: U.S. Geological Survey Professional Paper 1350, v. 2, p. 1019–1185.

Linker, M.F., and Dieterich, J.H., 1992, Effects of variable normal stress on rock friction; observations and constitutive equations: Journal of Geophysical Research, v. 97, no. B4, p. 4923–4940.

Nakamura, Kazuaki, 1982, Why do long rift zones develop in Hawaiian volcanoes—a possible role of thick oceanic sediments, *in* Schmincke, H.-U., Baker, P.E., and Forjaz, V.H., eds., Activity of ocean volcanoes, International Symposium on the Activity of Oceanic Volcanoes, July 1982, Proceedings: Ponta Delgada, Universidade dos Azores, Serie Ciencias da Naturezam, no. 3, p. 59–73.

Okamura, A.T., Dvorak, J.J., Koyanagi, R.Y., and Tanigawa, W.R., 1988, Surface deformation during dike propagation, chap. 6 *of* Wolfe, E.W., ed., The Puu Oo eruption of Kilauea Volcano, Hawaii; episodes 1 through 20, January 3, 1983, through June 8, 1984: U.S. Geological Survey Professional Paper 1463, p. 165–182.

Okubo, P.G., Benz, H.M., and Chouet, B.A., 1997, Imaging the crustal magma sources beneath Mauna Loa and Kilauea volcanoes, Hawaii: Geology, v. 25, no. 10, p. 867–870.

Owen, S.E., Segall, Paul, Freymueller, J.T., Miklius, Asta, Denlinger, R.P., Árnadóttir, Thóra, Sako, M.K., and Bürgmann, R.B., 1995, Rapid deformation of the south flank of Kilauea volcano, Hawaii: Science, v. 267, no. 5202, p. 1328–1332.

Pollard, D.D., Delaney, P.T., Duffield, W.A., Endo, E.T., and Okamura, A.T., 1983, Surface deformation in volcanic rift zones: Tectonophysics, v. 94, no. 1–4, p. 541–584.

Rubin, A.M., Gillard, Dominique, and Got, J.-L., 1998, A reinterpretation of seismicity associated with the January 1983 dike intrusion at Kilauea Volcano, Hawaii: Journal of Geophysical Research, v. 103, no. B5, p. 10003–10015.

Scholz, C.H., 1998, Earthquakes and friction laws: Nature, v. 391, no. 6662, p. 37–42.

Segall, Paul, and Matthews, M.V., 1988, Displacement calculations from geodetic data and the testing of geophysical deformation models: Journal of Geophysical Research, v. 93, no. B12, p. 14954–14966.

Simpson, R.W., and Reasenberg, P.A., 1994, Earthquake-induced static-stress changes on central California faults, *in* Simpson, R.W., ed., The Loma Prieta, California earthquake of October 17, 1989; tectonic processes and models: U.S. Geological Survey Professional Paper 1550–F, p. 55–89.

Stein, R.S., 1999, The role of stress transfer in earthquake occurrence: Nature, v. 402, no. 6762, p. 605–609.

Swanson, D.A, Duffield, W.A., and Fiske, R.S., 1976, Displacement of the south flank of Kilauea Volcano; the result of forceful intrusion of magma into the rift zones: U.S. Geological Survey Professional Paper 963, 39 p.

Thurber, C.H., and Gripp, A.E., 1988, Flexure and seismicity beneath the south flank of Kilauea volcano and tectonic implications: Journal of Geophysical Research, v. 93, no. B5, p. 4271–4278.

Tse, S.T., and Rice, J.R., 1986, Crustal earthquake instability in relation to the depth variation of frictional properties: Journal of Geophysical Research, v. 91, no. B9, p. 9452–9472.

Wolfe, E.W., Garcia, M.O., Jackson, D.B., Koyanagi, R.Y., Neal, C.A., and Okamura, A.T., 1987, The Puu Oo eruption of Kilauea Volcano, episodes 1–20, January 3, 1983, to June 8, 1984, chap. 17 Decker, R.W., Wright, T.L., and Stauffer, P.H., eds., Volcanism in Hawaii: U.S. Geological Survey Professional Paper 1350, v. 1, p. 471–508.

Wright, T.L., and Fiske, R.S., 1971, Origin of differentiated and hybrid lavas of Kilauea Volcano, Hawaii: Journal of Petrology, v. 12, no. 1, p. 1–65.